

# Addressing Factors Affecting Fluorescent Signal Collection of a Multimode Photonic Crystal Fiber Fluorometer

Jianjun Ma and Wojtek J. Bock, *Fellow, IEEE*

**Abstract**—A multimode photonic crystal fiber (PCF) fluorometer interrogated by a spectrometer is investigated. By adding a glass tip at the end of the PCF, we found that this fluorometer significantly enhances the fluorescent light collection efficiency (CE). Factors associated with the CE and stray light rejection are addressed. The experimental study verifies the proposed PCF probe based on the consideration of solely meridian rays. However, our further study in this paper shows the significance of skew rays under total internal reflection (TIR), which in fact carry 53% of the total guidable fluorescent signal power and are blocked in our experiment. We highlight that this missing power is strongly associated with the numerical aperture (NA) of each optical component in the system and suggest further improvement on the components in the system. The proposed PCF fluorometer is particularly efficient and cost effective for an immersion medium with a high attenuation.

**Index Terms**—Fiber characterization, fiber-optic sensors, fluorescence, luminescence, photonic crystal fiber (PCF), spectroscopy.

## I. INTRODUCTION

A TWO-FIBER or multifiber fluorometer with the fibers arranged side by side is often preferred as a measurement tool for chemical, biomedical, and clinical applications. The well-known advantages of such a device include small size, low cost, flexibility, and ease in accessing hard-to-reach places, as well as the long-distance remote monitoring capability. Maximizing the fluorescent light collection efficiency (CE) is a major concern. Different fiber tip designs for CE enhancement based on conventional multimode fibers, including an angled position of the fibers [1], beveled tips [2], [3], and a glass rod in front of the probe [4], have been proposed. However, it is difficult to further reduce the dead zone in front of the probe resulting from fiber claddings when conventional fibers are used. In particular, for a liquid sample with high attenuation, converting the dead zone to an active volume is highly desirable because of its proximity to the fiber probe front end, where both excitation and emission light will experience much less

Manuscript received July 5, 2007; revised June 19, 2008. First published July 25, 2008; current version published November 12, 2008. This work was supported by the Natural Sciences and Engineering Research Council of Canada. The Associate Editor coordinating the review process for this paper was Dr. Richard Thorn.

The authors are with the Centre de Recherche en Photonique, Département d'Informatique et d'Ingénierie, Université du Québec en Outaouais, Gatineau, QC J8X 3X7, Canada (e-mail: ma.jianjun@uqo.ca; wojtek.bock@uqo.ca).

Color versions of one or more of the figures in this paper are available online at <http://ieeexplore.ieee.org>.

Digital Object Identifier 10.1109/TIM.2008.928407

attenuation. To overcome this barrier, we have proposed using a large-core and multimode photonic crystal fiber (PCF), with pure silica material for both core and cladding, to build a fiber probe that will enhance the CE [5]. Significantly different from other existing approaches, this technique overcomes the dead zone by directly forming a pure glass tip through a one-step simple thermal fusion process [6]. The length of this glass tip has been demonstrated to have a dramatic impact on the CE. An associated theoretical model has previously been proposed and experimentally verified as well [11].

Further investigations—the main topic of this paper—emphasized other factors strongly affecting the collectable fluorescent signal. Often reported in publications, the analysis of the trajectory of mode or associated rays only considers meridian rays. In presenting a concept, it is clearly not possible to cover all possible mode groups or rays for CE enhancement. In fact, while the guiding mode group is certainly associated with meridian rays, a much greater number of guiding modes is formed by skew rays that also obey the total internal reflection (TIR) but never cross the fiber axis. They follow helical trajectories during their transmission in the fiber core and do not use the central area of the fiber core. Instead, they tend to use the area near the outer ring of the core for power delivery. A closed loop is observed when projecting one skew ray trajectory into the fiber core cross section. The effect of skew rays on the overall system performance will also strongly depend on the acceptance aperture and size of detector, as well as other components in the system, which will be discussed in this paper.

## II. THEORETICAL DESCRIPTION OF THE PROPOSED APPROACH

### A. Proposed Approach Based on Meridian Rays

The probe architecture is shown in Fig. 1. A conventional multimode fiber, i.e., model FIBER-300-SR with a pure silica core/cladding size of 300/330  $\mu\text{m}$  and an NA of 0.22 [7], is used as an illuminating fiber. Symmetrically surrounding it, two identical PCFs serve as the receiving fibers. The PCF (model MM-HNA-200) has a core/cladding size of 200/335  $\mu\text{m}$  and a high NA of 0.64 [8]. A ring of air holes surrounding the fiber core ensures the guiding condition of the PCF. As indicated in Fig. 1(a), three fiber probes are created, with PCF-1 as the first receiving fiber and PCF-2, PCF-3, or PCF-4 as the second receiving fiber. For technical reasons indicated later, PCF-1 has a very short glass tip to represent a PCF with open cladding

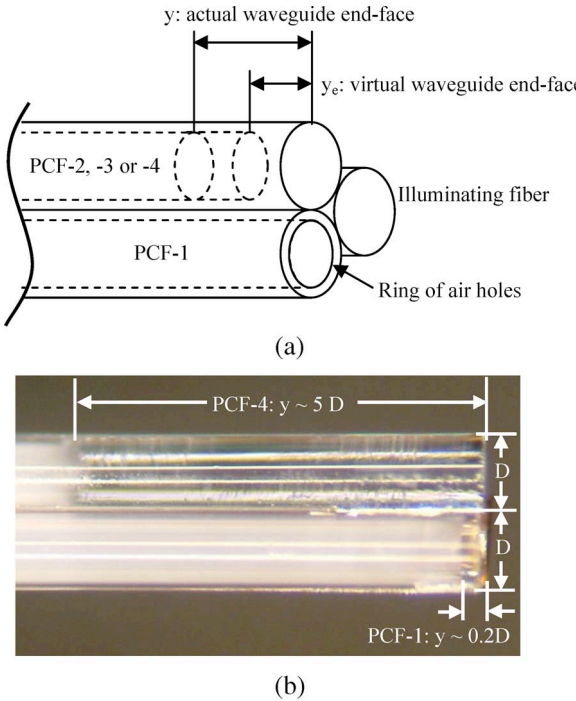


Fig. 1. PCF fiber fluorometer architecture for performance investigation. (a) Architecture of the probe end face. (b) Side view of the probe with PCF-1 and PCF-4 as receiving fibers.

holes. Fig. 1(b) shows a photograph of one probe, where the glass tips are clearly indicated. To facilitate analysis, Fig. 2(a) shows the four PCFs on one side of the illuminating fiber. A layer of polymer film sample [9] is cast on a glass substrate and placed in front of the probe at a distance  $d$ . The substrate is tilted to reduce the reflection of the stray excitation light.

The maximum acceptance angle of the spectrometer, which is associated with meridian rays and represented by  $\alpha$ , must completely be filled to simultaneously achieve stray excitation light rejection and maximum spectral resolution [10]. Therefore, extended from [11], the following relationship exists:

$$y = y_e \sqrt{\frac{n_2^2 - \sin^2 \alpha}{n_1^2 - \sin^2 \alpha}} \quad (1)$$

where  $y$  is the length of the glass tip, and  $y_e$  represents the separation between the virtual PCF tip face and the actual tip face. This separation is filled with a medium with a refractive index of  $n_1$  but no attenuation. This virtual PCF and its relationship with the actual glass tip are indicated in Fig. 1(a). With  $n_1 = 1$ ,  $n_2 = 1.46$ , and  $\alpha = \sin^{-1} 0.22 = 13^\circ$ , which is the maximum acceptance angle of the spectrometer in our investigation [6], (1) leads to  $y = 1.48y_e$ . Several typical lengths of virtual PCFs are further highlighted as PCF-1 ( $y_{e1}$ ), PCF-2 ( $y_{e2}$ ), PCF-3 ( $y_{e3}$ ), and PCF-4 ( $y_{e4}$ ) in Fig. 2(a), representing, respectively, a separation of zero (approximately), the separation determined by matching  $\alpha$  with the fiber cladding thickness, the separation for maximum CE, and the separation for full elimination of stray light. For PCF-2, we have

$$y_e = (R - r) \operatorname{ctg} \alpha \quad (2)$$

where  $R$  and  $r$  are the radii of the PCF cladding and core, respectively. The calculation shows that  $y_{e2} = 292 \mu\text{m}$  or  $y = 432 \mu\text{m} = 1.29D$ . We expect PCF-2 to have a better CE than PCF-1. However, as indicated in Fig. 2(a), ray A'A, having a wide range of possible angles from  $\alpha = 13^\circ$  to  $40^\circ$ , will be guided by the PCF due to its very high numerical aperture ( $NA_r = 0.64$ ) and will generate stray light rays. Additionally, at this position, some rays with smaller incident angles and higher fluorescent intensity, represented by the ray B'B, will be blocked. This implies that the optimized tip length  $y$  associated with maximum CE should be somewhere beyond  $y_{e2}$ . The position of PCF-4 is determined in such a way that ray C'C at  $\alpha = 13^\circ$  in Fig. 2(a) hits the cladding across the core, that is

$$y_{e4} = (R + r) \cdot \operatorname{ctg} \alpha. \quad (3)$$

For the PCF used here, (3) leads to  $y_{e4} = 1159 \mu\text{m}$  or  $y = 5.1 D$ , where all the received emitted rays fall within  $\alpha$ . However, this position usually does not create the maximum CE. Our ray tracing indicates that although at this position the CE for very small angle rays is improved, the CE for rays with larger incident angles from the same spot is enormously reduced, leading to a dramatic drop in the overall signal level. To further disclose the relationship among those factors associated with CE and facilitate the probe fabrication, we propose a simplified model based on an all-conventional-fiber probe. This probe, as shown in Fig. 2(b), includes the same type of illuminating fiber (without jacket) and receiving fiber (with jacket), which has a core/cladding/jacket size of 300/330/650 and an NA of 0.37. For this probe, the front area of the receiving fiber is filled with air, leading to  $y_e = y$ . The experimental result indicated in [12] shows that the maximum CE is found when  $y_e = 2 \text{ mm}$  and at  $d = 2.75 \text{ mm}$ . Further ray tracing indicates that the maximum CE is achieved when ray A'A meets several conditions. First, it must be launched from the intersection point of the sample surface and the axis of the illuminating fiber, which is always occupied by the peak of the Gaussian-shaped intensity profile. Second, this ray has to have an optimum incident angle  $\gamma$  and has to hit the center of the receiving fiber. This optimum angle  $\gamma$  for maximum CE can be expressed by a general formula applicable to any fiber size as

$$\gamma = \operatorname{tg}^{-1} \left( \frac{R_{\text{ill}} + R}{d + y_e + (2R + R_{\text{ill}}) \cdot \operatorname{tg} \delta} \right) \quad (4)$$

where  $R_{\text{ill}}$  and  $\delta$  are the cladding radius of the illuminating fiber and the tilted angle of the sample ( $\delta = 37^\circ$  in our experiment), respectively.

From the experimental result for this probe, (4) gives  $\gamma = 5^\circ$ . Roughly speaking, this falls within the middle range of angles between  $0^\circ$  and  $13^\circ$ , which is the range of incident angles allowed by the spectrometer. Using a ray with this incident angle to determine  $y_e$ , further ray tracing shows that other rays with larger and smaller incident angles than  $\gamma$  and emitted from the sample areas with strong excitation are also accepted by the receiving fiber. This implies that the angle  $\gamma$  can be approximately determined by the maximum acceptance angle of the spectrometer  $\alpha$ . With the same spectrometer, for other

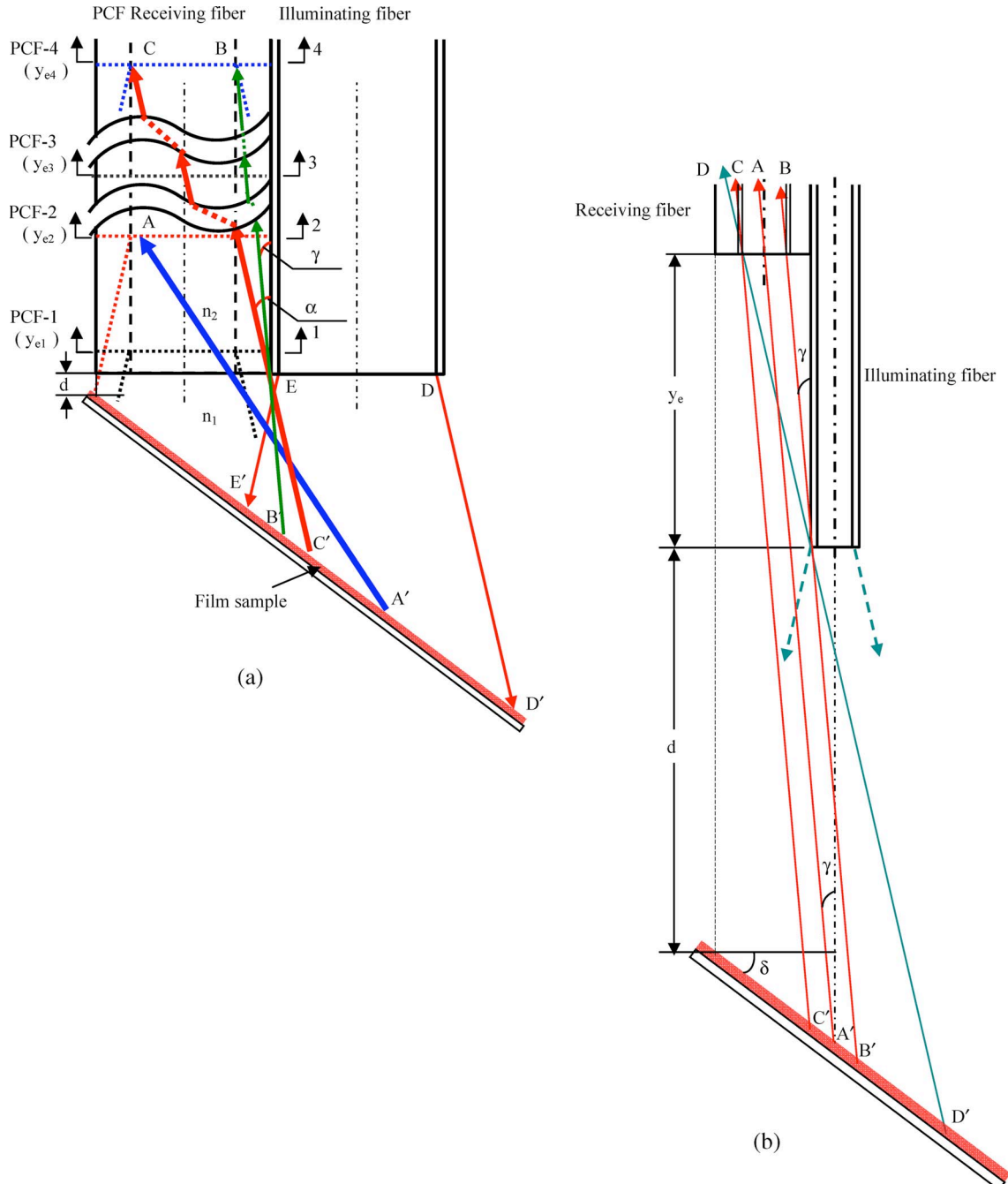


Fig. 2. Investigation of probes for optimized PCF glass tip. (a) Probe with different lengths of glass tips. (b) An all-conventional-fiber probe illustrating the parameters associated with CE.

fiber core/cladding and/or jacket sizes, it is, therefore, valid to use  $\gamma = 5^\circ$  to calculate  $y$  or  $y_e$ , which is given by

$$y_e = (R - r) \cdot ctg\gamma. \quad (5)$$

Equation (5) is actually an additional condition for (4), further restricting the relation between  $d$  and  $y_e$  and ensuring that the ray with  $\gamma = 5^\circ$  emitted from the vicinity of the Gaussian peak will be received. Simply applying (5) to the case of the PCF probe, we have  $y_e = 771 \mu\text{m}$  or  $y = 3.4 D$ , which is the predicted length of the glass tip for maximum CE. Although this maximum CE is achieved by introducing some stray light,

we notice that it is also associated with a longer sample distance  $d$ . As a result, the rays of stray light, which are represented by ray D'D in Fig. 2(b), are emitted from areas far from the center of the Gaussian-shaped profile, causing no observable reduction of the signal-to-noise ratio.

#### B. Significant Effect of Skew Rays on System Performance

As indicated in Section I, rays traveling in the core as part of the TIR fall into one of two categories: meridian rays or skew rays, both of which are associated with guiding modes. Most discussions appearing in the literature concentrate on meridian

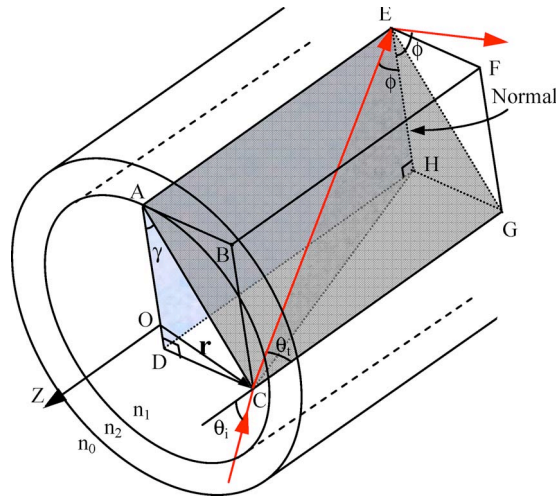


Fig. 3. Analysis of skew ray formation at position  $r$  under TIR.

rays and disregard skew rays. The fact is, however, that most of the guiding modes are formed by the congruence of skew rays. Their effect on system performance is thus significant.

A widely accepted concept of the maximum acceptance angle of a multimode fiber, which is determined by NA with  $2\alpha = 2 \sin^{-1} \text{NA}$ , is in fact only applicable to meridian rays. According to this concept, all rays falling within the cone of  $2\alpha$  are meridian rays and have also been used in Section II-A. The incident angles capable of exciting meridian rays are thus

$$0 < \theta_{\text{mdn}} \leq \sin^{-1} \text{NA}. \quad (6)$$

Under TIR, skew rays follow a trajectory located off the core center  $O$ . One such ray shown in Fig. 3, lying in the plane ACGE, has an angle  $\gamma$  with the meridian plane ADHE, where meridian rays are found. From the geometry in Fig. 3, the following relationship exists under the assumption of TIR:

$$\cos \gamma \cdot \sin \theta_t = \cos \phi = \sqrt{1 - \frac{n_2^2}{n_1^2}}. \quad (7)$$

The general requirement governing the incident angle  $\theta_{\text{skw}}$  of skew rays can, hence, be simply derived from Snell's law as

$$n_0 \sin \theta_{\text{skw}} \geq \frac{\sqrt{n_1^2 - n_2^2}}{\cos \gamma} = \frac{NA_{\text{mdn}}}{\cos \gamma} \geq NA_{\text{mdn}} \quad 0 < \gamma < \frac{\pi}{2}. \quad (8)$$

So the numerical aperture of meridian rays is only the special case of (8) when  $\gamma = 0$ . Clearly,  $\theta_{\text{skw}} \geq \theta_{\text{mdn}}$ , suggesting that the minimum incident angle of skew rays starts from the maximum acceptance angle of meridian rays. In other words, the guiding modes associated with skew rays can only be excited by rays outside the maximum acceptance cone of meridian rays, including rays with incident angles close to  $\pi/2$ . Furthermore, from Fig. 3, each meridian plane is associated with many skew planes since  $\gamma$  can vary within a wide range

of values. Obviously, then, there are far more skew rays than meridian rays in a multimode fiber waveguide.

With the above analysis in mind, referring to Fig. 2(a), one of the important attributes of fluorescent emission occurring in the illuminated area  $E'D'$  is that each differential area  $dA$  behaves like a diffuse source. The emission rays launched from it will randomly propagate in all directions above the sample with identical strength. Some rays hit the PCF-receiving fiber entrance by obeying (8), creating skew rays propagating inside the core. However, the number of skew rays is affected in a more complex way than the meridian rays. The first factor, which is similar to meridian rays, is the separation between the PCF-receiving fiber and the sample. An optimized distance  $d = d_{\text{OP\_skw}}$  exists for the highest power solely carried by skew rays. The same result holds for meridian rays with  $d = d_{\text{OP\_mdn}}$ . However, usually,  $d_{\text{OP\_skw}} \neq d_{\text{OP\_mdn}}$ . If we fix the PCF-receiving fiber position, for instance, the position of PCF-1, we might expect that the overall received signal will be determined by a position between  $d_{\text{OP\_skw}}$  and  $d_{\text{OP\_mdn}}$ . This is only true when the detector is also unchanged. In fact, to accept skew rays, the detector needs a wider acceptance angle since the entrance angle of a skew ray, obeying (8), is identical to the exit angle at the detector end when the waveguide is ideal. When a spectrometer is chosen, its designated acceptance angle, slit width, and height will affect skew rays more significantly than meridian rays. Using an alternative means of detection, such as an optical detector with a large light acceptance area close to the fiber exit, or adding a collimating or focusing lens with a large numerical aperture in between might help to collect more fluorescent signal.

### III. EXPERIMENTS AND RESULTS

To reduce the measurement error during the experiments, all PCFs must have the same tip surface flatness. This is achieved by polishing the tip surfaces under the same conditions. To do this, the air holes at the distal end of PCF-1 are sealed over a very short length ( $y_1 \sim 0.2 \text{ D}$ ) to prevent contamination. This process is done by using a fusion splicer. Since the PCF we used has a large core/cladding size of  $200/335 \mu\text{m}$ , a regular automatic fusion splicer for standard fiber communication purpose will not work. A semi-automatic portable fiber splicer (model PFS 330 from Power Technology Inc.) was used to achieve the best fusing result. The arc time and current must manually be adjusted, combined with manually feeding the PCF end to the discharge electrodes. Each cladding hole has a tiny size of around several micrometers, which is much smaller than the fiber core size of  $200 \mu\text{m}$ , so there is no observable change of fiber outer diameter after the fusion process, as indicated in Fig. 1(b). From (1), the corresponding equivalent virtual tip end position of PCF-1 is  $y_{e1} \sim 44 \mu\text{m}$ . In fact, such a tiny separation falls within the tolerance of alignment error during the probe preparation. So we use PCF-1 to represent the PCF with open holes and set it flush with the illuminating fiber. In accordance with the analysis in Section II-A, the pure glass tips of PCF-2, PCF-3, and PCF-4 are created with lengths of  $y_2 \sim 1.28D$ ,  $y_3 \sim 3D$ , and  $y_4 \sim 5D$ , respectively. Ideally, the four PCFs would be placed around the illuminating fiber to

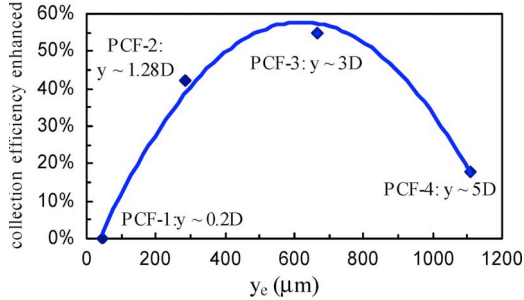


Fig. 4. Experimental result of fluorescent signal level enhancement for different lengths of glass tip. The unit of intensity is based on the sensitivity of the USB2000 spectrometer at 86 photons/count (estimate).

maintain the same illuminating conditions. However, due to the technical difficulties of accurately controlling the lengths of all four PCF glass tips simultaneously during the polishing process, we separately prepared three probes with the architecture shown in Fig. 1(a). These three probes share the same PCF-1 and the same illuminating fiber to facilitate comparison between the probes. Neither the PCF nor the illuminating fiber showed any observable bending losses, which is a fact that minimizes the measurement error associated with the fiber-bending effect. The first probe with PCF-2 was disassembled once the data-collection process was completed. The second probe was prepared by simply replacing PCF-2 with PCF-3. The same procedure was repeated for the third probe with PCF-4. All probes were carefully prepared under a microscope.

A linear variable filter [7] was carefully adjusted to reject stray excitation light and to allow the fluorescent light to pass through. One port of the filter holder is connected with a fiber patch cord, whereas another is connected with the PCF-receiving fiber. The fiber patch cord, having a 400- $\mu\text{m}$  core diameter and a NA of 0.22, guarantees maximum light coupling from the PCF and ensures that the acceptance angle of the Ocean Optics USB2000 spectrometer is met [7]. A computer with OOIbase32 Spectrometer Operating Software communicates with the USB2000 and performs all the necessary data saving and processing. To maximize the fluorescent signal level, the probe-to-sample separation and the laser diode-to-fiber coupling can be adjusted through a precision translation stage and a fiber positioner, respectively. The film sample is excited by a laser diode (maximum 3-mW output power without pigtail fiber) at 532 nm delivered by the illuminating fiber and then emits at 640 nm (central wavelength). Before the experiment, the fluctuation of the excitation light after the illuminating fiber is monitored by connecting it to an HP 8152A power meter. Within 1 hour, the fluctuation is below 5%, which is considered acceptable.

During the experiment, an identical film sample with a thickness of  $\sim 4.7 \mu\text{m}$  was used for all PCF fiber probes. The laboratory environment maintains the same room temperature and humidity, ensuring that all results were achieved under the same sample condition. Fluorescence fluctuation on the captured spectrum was observed, however, with a percentage of only about 0.2%, which is considered to be negligible based on the following experimental results. These results are illustrated in Fig. 4, indicating that the PCF-2 probe, with a 44% increase

of CE, does not show the maximum CE. However, maximum enhancement is observed for the PCF-3 probe ( $y \sim 3D$ , close to the predicted glass tip length  $y = 3.4D$ ), which is 55% higher than would be achieved by PCF-1. For the PCF-4 probe whose glass tip has a length of  $5D$ , which is close to the length capable of stray light rejection, we observed a significantly reduced signal level and a much lower CE enhancement of only 18%. Moreover, no obvious signal quality deterioration is observed for the PCF-3 probe in comparison with the PCF-4 probe, confirming the negligible effect of stray light.

#### IV. FURTHER DISCUSSION OF THE EXPERIMENTAL RESULTS

In general, the experiments described in Section III show that the meridian rays are sufficient for the proposed probe design since the results prove the discussion in Section II-A. However, this result is due to the fact that there are several bottlenecks in the system, blocking the power carried by the large number of skew rays. As indicated in Section II-B, within the system, the PCF with  $\text{NA} = 0.64$  has more qualified guiding modes than the fiber patch cord with  $\text{NA} = 0.22$  and core diameter of 400, although the PCF only has a 200- $\mu\text{m}$  core. The mode number ratio  $\Gamma$  is calculated by

$$\Gamma = \frac{N_{\text{Pcord}}}{N_{\text{PCF}}} = \left( \frac{V_{\text{Pcord}}}{V_{\text{PCF}}} \right)^2 = \left( \frac{r_{\text{Pcord}} N_{\text{A Pcord}}}{r_{\text{PCF}} N_{\text{A PCF}}} \right)^2 = 47\% \quad (9)$$

where

$N_{\text{Pcord}}$  and  $N_{\text{PCF}}$  number of guiding modes in the fiber patch cord and the PCF, respectively;

$V_{\text{Pcord}}$  and  $V_{\text{PCF}}$  normalized frequencies of the respective fibers;

$r_{\text{Pcord}}$  and  $r_{\text{PCF}}$  fiber core diameters of the respective fibers.

Equation (9) indicates that about 53% of the guiding modes in the PCF-receiving fiber, which are qualified to carry signal power, are blocked at the entrance of the fiber patch cord, and most of them are associated with skew rays. Moreover, the FH-LVF itself includes a pair of collimating lenses to transfer power from the PCF to the patch cord. These lenses have limited light-acceptance angles and are another source of power blockage. The eventual power delivered to the entrance of the spectrometer is determined by the NAs of both the lenses and the patch cord as well as the allowed mode volume  $N_{\text{Pcord}}$  if the material of all the components is attenuation free. This remaining power will experience further loss due to the limitation of the spectrometer entrance slit, as highlighted in Section II-B. Fortunately, the USB2000 spectrometer in this experiment is designed to fit the NA of the patch cord (0.22), and the fiber core itself is the slit. All remaining power is able to fully enter the spectrometer. This remaining power is considered to come from only the meridian rays since the NA of the collimating lens and its limited aperture will remove most of the skew rays launched from the PCF. The match between Sections II-A and III, where only meridian rays are considered, becomes natural.

## V. CONCLUSION

In conclusion, we have proved that a multimode PCF with a seamlessly integrated front glass tip has the ability to enhance fluorescent CE and/or reject stray light. A theoretical model for probe performance prediction associated with such tips is established and fully verified via experiments. With further emphasis on skew ray group, which is supposed to be able to carry more signal power, we have discussed the condition of skew ray formation and associated key elements in the entire measurement system. The discussion also indicates how to further enhance system performance by improving such elements as the lens and detection means.

The proposed PCF fluorometer is highly efficient, cost effective, and compact. Moreover, when used in a liquid sample characterized by a high attenuation, as in the case of wastewater monitoring and underwater explosive detection, this glass tip, with zero attenuation, offers another unique advantage: It could replace the volume occupied by the liquid immersion medium when employing a conventional fiber and, thus, greatly reduces the overall signal loss in the system.

## REFERENCES

- [1] P. Plaza, Q. D. Nguyen, M. Jouan, H. Fevrier, and H. Saisse, "Simulation et optimisation des capteurs à fibres optiques adjacentes," *Appl. Opt.*, vol. 25, no. 19, pp. 3448–3454, Oct. 1986.
- [2] T. F. Cooney, H. T. Skinner, and S. M. Angel, "Comparative study of some fiber-optic remote Raman probe designs—Part I: Model for liquids and transparent solids," *Appl. Spectrosc.*, vol. 50, no. 7, pp. 836–848, Jul. 1996.
- [3] T. F. Cooney, H. T. Skinner, and S. M. Angel, "Comparative study of some fiber-optic remote Raman probe designs—Part II: Tests of single-fiber, lensed, and flat- and bevel-tip multi-fiber probes," *Appl. Spectrosc.*, vol. 50, no. 7, pp. 849–860, Jul. 1996.
- [4] U. Utzinger and R. R. Richards-Kortum, "Fiber optic probes for biomedical optical spectroscopy," *J. Biomed. Opt.*, vol. 8, no. 1, p. 121, Jan. 2003.
- [5] J. Ma and W. J. Bock, "Photonic crystal fiber fluorometer: Consideration of factors associated with maximum fluorescent collection," in *Proc. IEEE IMTC*, Warsaw, Poland, 2007, pp. 1–4.
- [6] W. J. Bock and J. Ma, U. S. Patent 2007/0230859 A1, Apr. 2, 2007.
- [7] [Online]. Available: <http://www.oceanoptics.com/homepage.asp>
- [8] *Multimode ultra high NA photonic crystal fiber-MM HN 200* (MM HNA 200 Rev 2.0 Oct. 2003). [Online]. Available: <http://www.crystal-fibre.com/datasheets/MM-HNA-200.pdf>

- [9] S. M. MacKinnon and Z. Y. Wang, "Synthesis and characterization of poly(aryl ether imide)s containing electroactive perylene diimide and naphthalene diimide units," *J. Polym. Sci., A, Polym. Chem.*, vol. 38, no. 19, pp. 3467–3475, 2000.
- [10] W. Demtröder, *Laser Spectroscopy: Basic Concepts and Instrumentation*, 2nd ed. Berlin, Germany: Springer-Verlag, 1996, ch. 4.
- [11] J. Ma and W. J. Bock, "Modeling of photonic crystal fiber with air holes sealed at the fiber end and its application to fluorescent light collection efficiency enhancement," *Opt. Express*, vol. 13, no. 7, pp. 2385–2393, Apr. 2005.
- [12] J. Ma, W. J. Bock, Z. Wang, and W. Hao, "Towards optimum sample-probe-spectrometer system design by adjusting receiving fiber end face position and probe-membrane sample separation," *Opt. Express*, vol. 13, no. 23, pp. 9492–9501, Nov. 2005.

**Jianjun Ma** received the Ph.D. degree in electrophysics and optoelectronics from Zhejiang University, Hangzhou, China, in 1996.

From 1998 to 2000, he was a Research Fellow with Nanyang Technological University, Singapore, where he continued his research on fiber-optic sensors for smart structures. Since 2000, he has been a Research Scientist with the Centre de Recherche en Photonique, Département d'Informatique et d'Ingénierie, Université du Québec en Outaouais, Gatineau, QC, Canada. His research involves novel fiber-optic sensing technology investigation, data-acquisition system configuration, and software programming for interrogating specifically designed fiber-optic sensors. His current research area covers fiber-optic sensors for chemical, biomedical, and clinical applications.



**Wojtek J. Bock** (M'85–SM'90–F'03) received the M.Sc. degree in electrical engineering and the Ph.D. degree in solid-state physics from Warsaw University of Technology, Warsaw, Poland, in 1971 and 1980, respectively.

He is currently a Full Professor of electrical engineering and a Canada Research Chair in photonics with the Université du Québec en Outaouais, Gatineau, QC, Canada, where he is also the Director of the Centre de Recherche en Photonique. He has authored and coauthored more than 250 scientific papers, patents, and conference proceedings in the fields of fiber optics and metrology. His research interests include fiber-optic sensors and devices, multisensor systems, and precise measurement systems of nonelectric quantities.

Dr. Bock was a member of the Administrative Committee of the IEEE Instrumentation and Measurement Society for eight years. He was the General Chairman of the IEEE Instrumentation/Measurement Technology Conference (IMTC/97), Ottawa, ON, Canada, May 1997.